Equatorial Western-Central Pacific SST Responsible for the North Pacific Oscillation-ENSO Sequence®

Suqiong Hu, a Wenjun Zhang, a Masahiro Watanabe, b Feng Jiang, a Fei-Fei Jin, c and Han-Ching Chen a

^a Key Laboratory of Meteorological Disaster, Ministry of Education (KLME), Joint International Research Laboratory of Climate and Environment Change (ILCEC), Collaborative Innovation Center on Forecast and Evaluation of Meteorological Disasters,

Nanjing University of Information Science and Technology, Nanjing, China

^b Atmosphere and Ocean Research Institute, The University of Tokyo, Kashiwa, Japan

(Manuscript received 17 July 2023, in final form 12 February 2024, accepted 27 February 2024)

ABSTRACT: El Niño-Southern Oscillation (ENSO), the dominant mode of interannual variability in the tropical Pacific, is well known to affect the extratropical climate via atmospheric teleconnections. Extratropical atmospheric variability may in turn influence the occurrence of ENSO events. The winter North Pacific Oscillation (NPO), as the secondary dominant mode of atmospheric variability over the North Pacific, has been recognized as a potential precursor for ENSO development. This study demonstrates that the preexisting winter NPO signal is primarily excited by sea surface temperature (SST) anomalies in the equatorial western-central Pacific. During ENSO years with a preceding winter NPO signal, which accounts for approximately 60% of ENSO events observed in 1979-2021, significant SST anomalies emerge in the equatorial western-central Pacific in the preceding autumn and winter. The concurrent presence of local convection anomalies can act as a catalyst for NPO-like atmospheric circulation anomalies. In contrast, during other ENSO years, significant SST anomalies are not observed in the equatorial western-central Pacific during the preceding winter, and correspondingly, the NPO signal is absent. Ensemble simulations using an atmospheric general circulation model driven by observed SST anomalies in the tropical western-central Pacific can well reproduce the interannual variability of observed NPO. Therefore, an alternative explanation for the observed NPO-ENSO relationship is that the preceding winter NPO is a companion to ENSO development, driven by the precursory SST signal in the equatorial western-central Pacific. Our results suggest that the lagged relationship between ENSO and the NPO involves a tropical-extratropical two-way coupling rather than a purely stochastic forcing of the extratropical atmosphere on ENSO.

KEYWORDS: Atmosphere-ocean interaction; ENSO; North Pacific Oscillation; Interannual variability

1. Introduction

El Niño-Southern Oscillation (ENSO) is an ocean-atmosphere mode in the equatorial Pacific, characterized by the interannual fluctuations between warm (El Niño) and cold (La Niña) sea surface temperature (SST) anomalies in the central and eastern equatorial Pacific and the corresponding coupled changes in zonal sea level pressure gradient (Bjerknes 1969; Neelin et al. 1998; Philander 1985). It is the most energetic variation of the climate system and the primary source of seasonal-to-interannual climate predictability on Earth. Although ENSO originates and develops mainly in the tropical Pacific, it can affect global weather and climate anomalies through so-called atmospheric teleconnections (e.g., Alexander et al. 2002; Ropelewski and Halpert 1987; Lau 1997; van Loon and Madden 1981). Over the past few decades, much attention has been paid to understanding its dynamics and potential predictability (e.g., Jin 1997a,b; Cane and Zebiak 1985; Neelin et al. 1998). It is widely recognized that the growth of

Corresponding author: Wenjun Zhang, zhangwj@nuist.edu.cn

ENSO SST involves a positive ocean–atmosphere feedback between the equatorial zonal winds and east–west SST gradient (i.e., the Bjerknes feedback) (Bjerknes 1969). The ENSO oscillatory behavior is tied to the meridional displacement of subsurface warm water toward and away from the equator, as demonstrated by the classic recharge oscillator (RO) paradigm (Jin 1997a,b). According to the RO theory, the warm water volume (WWV) in the equatorial Pacific could be used as a key ENSO predictor since the WWV anomaly usually leads the ENSO SST anomaly by about two to three seasons (McPhaden 2003; Meinen and McPhaden 2000).

However, the phase-lag relationship between the WWV and ENSO SST underwent a notable decadal shift from two to three seasons prior to 2000 to one season after 2000 (e.g., McPhaden 2012; Bunge and Clarke 2014; Bosc and Delcroix 2008), possibly contributed by the more frequent occurrence of central Pacific ENSO events in the past two decades (Zhang et al. 2019; Zhao et al. 2021). Correspondingly, the predictability of ENSO SST has decreased to only one season after the year 2000 (Kumar et al. 2015; Wang et al. 2010; Hendon et al. 2009). In addition to focusing on the processes local to the tropical Pacific, there is also a suggestion that atmospheric and ocean variability outside this area may contribute to shaping ENSO evolution and enhancing its predictability (e.g., Vimont et al. 2001, 2003b; Anderson 2003; Nakamura et al. 2006; Terray 2011; You and Furtado 2018).

^c Department of Atmospheric Sciences, School of Ocean and Earth Science and Technology, University of Hawai'i at Mānoa, Honolulu, Hawaii

Supplemental information related to this paper is available at the Journals Online website: https://doi.org/10.1175/JCLI-D-23-0434.s1.

For example, the North Pacific meridional mode (NPMM) and South Pacific meridional mode (SPMM) have been proposed to act as an ocean bridge, linking the extratropical atmospheric variability to ENSO variability (You and Furtado 2018; Zhang et al. 2014; Chiang and Vimont 2004; Chang et al. 2007; You and Furtado 2017). These two meridional modes are suggested to contribute differentially to ENSO flavors (Pegion et al. 2020; Vimont et al. 2014; Yu and Kim 2011; You and Furtado 2017, 2018). The winter North Pacific Oscillation (NPO) (Rogers 1981; Walker and Bliss 1932), manifesting as a north-south seesaw in the sea level pressure (SLP) anomalies over the North Pacific, is argued to have the potential to improve ENSO prediction skill 1 year ahead beyond its spring predictability barrier (Chen et al. 2020; Tseng et al. 2022; Vimont et al. 2003a,b). A positive NPO event during boreal winter tends to be followed by an El Niño event in the following winter and a negative NPO event generally corresponds to the following La Niña winter. The anomalous winds associated with the winter NPO could impart an SST footprint similar to NPMM onto the ocean by altering the surface net heat flux through a process known as the seasonal footprinting mechanism (SFM) (Vimont et al. 2001, 2003b). This SST footprint persists into the following late spring and summer when its subtropical component could in turn force the overlying atmospheric circulation, and further, the accompanied equatorial zonal wind anomalies contribute to the development of the following ENSO events. It has been also argued that the NPO-related anomalous southwesterly winds over the subtropical North Pacific can generate simultaneous subsurface ocean temperature anomalies in the central and eastern equatorial Pacific. These anomalies could play a role in initiating subsequent ENSO events through a mechanism known as the trade wind charging (TWC) mechanism (Anderson 2004; Anderson et al. 2013). Moreover, recent studies proposed that the NPO could impact subsequent ENSO events via the propagation of upper-tropospheric wave energy (Zhao et al. 2023a,b). Notably, some studies argue that the role of NPO in initiating the following ENSO events strongly depends on the state of the tropical Pacific itself (Anderson 2007; Deser et al. 2012). When the winter NPO signal is accompanied by preceding summer/autumn subsurface temperature anomalies in the western tropical Pacific, its correlation with the following winter ENSO events becomes stronger. It is well established that tropical Pacific SST anomalies exert a significant influence on atmospheric variability over the North Pacific (Trenberth et al. 1998; Alexander et al. 2002). The impacts of these SST anomalies are intricate and depend on various factors, including their location, strength, and background state (e.g., Ashok et al. 2009; Hoell et al. 2016; Guo et al. 2017; Trascasa-Castro et al. 2023; Bayr et al. 2019). For example, it has been suggested that more westward ENSO SST anomalies tend to induce an atmospheric circulation anomaly resembling the NPO pattern (Di Lorenzo et al. 2010; Ding et al. 2022; Furtado et al. 2012).

This raises the question of whether the lagged relationship between the ENSO and the NPO involves a tropical–extratropical two-way coupling. It has been well established that NPMM could affect the following ENSO events (Chang et al. 2007; Amaya et al. 2019). Stuecker (2018) pointed out that the central Pacific ENSO could in turn generate an instantaneous NPMM response by initiating atmospheric teleconnection with a strong projection on the

Aleutian low. Similarly, if the preexisting winter NPO for ENSO years can be traced to the tropical Pacific itself, caution is warranted in determining whether it can offer additional predictive information for subsequent ENSO events beyond the commonly used tropical Pacific ocean-atmosphere conditions. In the present work, we investigate the possible tropical origin of the NPO signal in the preceding winter of ENSO years. Our analyses show that the preexisting winter NPO signal for ENSO events could be largely attributed to the equatorial western-central Pacific SST forcing. The rest of this paper is organized as follows. Section 2 describes the datasets, methods, and experimental designs. In section 3, we display the observed preceding winter SLP signal over the North Pacific for ENSO. Section 4 investigates the possible tropical origin of the preceding winter NPO signal for ENSO. The role of equatorial western-central SST in the NPO-ENSO sequence is addressed in section 5. Finally, we summarize the main conclusions and discuss related issues in section 6.

2. Data, methodology, and experimental designs

a. Data and methodology

The following datasets are employed in this study: 1) Monthly atmosphere data from the fifth major global reanalysis produced by European Centre for Medium-Range Weather Forecasts (ECMWF) (ERA5) dataset, with a horizontal resolution of $0.25^{\circ} \times 0.25^{\circ}$ (Hersbach et al. 2020). The reanalysis data utilized include SLP and horizontal wind at 10 m. 2) Monthly subsurface ocean temperature data on a 1° × 1° grid from ECMWF Ocean Reanalysis System 5 (ORAS5) (Zuo et al. 2019). 3) Monthly SST data derived from the Met Office Hadley Centre (Hadley Centre Sea Ice and Sea Surface Temperature dataset, Version 1, or HadISST1), with a horizontal resolution of $1^{\circ} \times 1^{\circ}$ (Rayner et al. 2003). 4) Monthly precipitation data on a $2.5^{\circ} \times 2.5^{\circ}$ grid from the Climate Prediction Center (CPC) Merged Analysis of Precipitation (CMAP) (Xie and Arkin 1996). Our analysis covers the period from January 1979 to December 2021 due to the constraints imposed by precipitation data from CMAP. Anomalies are obtained by removing the monthly mean climatology for the period of 1981-2010 and are linearly detrended to avoid the possible influences from the long-term trend. The SLP and SST data from 1940 to 2021 are also used to test the robustness of our results, and the qualitative conclusion remains consistent (Figs. S1-S3 in the online supplemental material). Our regression analysis is performed using the two-tailed Student's t test. The effective number of degrees of freedom $(N_{\rm eff} = N/T)$ is calculated to remove the influence of autocorrelation on the correlation significance (Davis 1976), where N denotes the sample size and $T = \sum_{j=-\infty}^{\infty} R_{xx}(j) R_{yy}(j)$, where $R_{xx}(j)$ and $R_{yy}(j)$ are the autocorrelation of two sample series at the lag time of j. We also employ a bootstrapped significance test for our composite analysis (Parnell 2013). Field significance is further conducted on our spatial fields according to the false discovery rate (FDR) method with $\alpha_{\rm FDR} = 0.1$ (Wilks 2006, 2016).

The Niño-3.4 index, SST anomalies averaged over 5°S–5°N and 120°–170°W, is used as a measure of ENSO variability. The cold tongue index (CTI) is defined as the averaged SST anomalies in the region of 6°S–6°N and 180°–90°W. ENSO

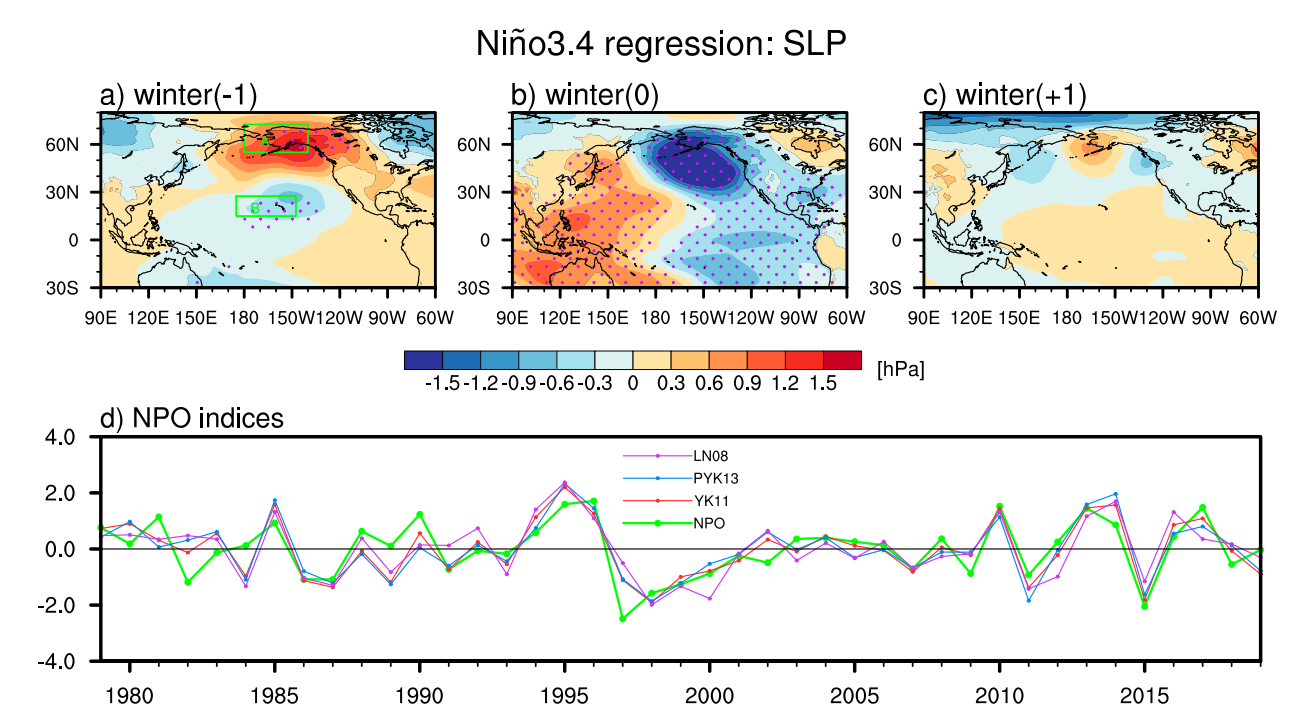


FIG. 1. Regression of SLP anomalies (shading; hPa) in the (a) preceding winter [winter(-1)], (b) simultaneous winter (winter(0)], and (c) subsequent winter [winter(+1)] upon the winter Niño-3.4 index. The two green boxes in (a) are the domains used to define the NPO index. Purple dots indicate regression coefficients that are statistically significant at the 95% confidence level. (d) Normalized time series of the winter NPO index and three NPO indices (YK11, PYK13, and LN08) defined based on the EOF method.

events are identified based on a threshold of 0.5 standard deviation of the winter (December-January-February) Niño-3.4 index. There are 12 El Niño (1982/83, 1986/87, 1987/88, 1991/92, 1994/95, 1997/98, 2002/03, 2006/07, 2009/10, 2014/15, 2015/16, and 2018/19) and 15 La Niña (1983/84, 1984/85, 1985/86, 1988/89, 1995/96, 1998/99, 1999/2000, 2000/01, 2005/06, 2007/08, 2008/09, 2010/11, 2011/12, 2017/18, and 2020/21) years during 1979–2021. Year(0)/year(1) represents the developing and decaying years of ENSO events, respectively. Following a previous definition (Furtado et al. 2012), the NPO index used in this study is calculated as the difference of the SLP anomalies between the box A (55°-72.5°N and 180°-220°E) and box B (15°-27.5°N and 175°-212.5°E) regions in Fig. 1a. Three NPO indices (i.e., YK11, PYK13, and LN08) based on empirical orthogonal function (EOF) analysis are adopted to compare with the used NPO index (Yu and Kim 2011; Park et al. 2013; Linkin and Nigam 2008). YK11, PYK13, and LN08 are used to represent the corresponding time series of the second EOF mode of the SLP anomalies over 120°E-80°W and 20°-60°N, 100°E-80°W and 0°-70°N, and 120°E-120°W and 20°-85°N, respectively. To investigate the role of equatorial western-central SST anomalies in the preceding winter NPO, the western Pacific SST index (WPI) is calculated as an area average of the SST anomalies in the region of 10°S-10°N and 150°-170°E. The subsurface ocean heat content (OHC) anomalies are calculated by averaging ocean temperature anomalies from 0 to 350 m. The meridional modes are defined by performing a maximum covariance analysis (MCA) on monthly mean SST and the 10-m wind components (You and Furtado 2018; Chiang and Vimont 2004;

Amaya et al. 2019). Prior to calculating the MCA, both the SST and wind data are preprocessed to remove the effects of long-term climate change (i.e., detrending) and to remove the influence of ENSO by linearly regressing out ENSO signal (CTI). The NPMM is derived as the first MCA mode (MCA1) of the cross-covariance matrix between SST and 10-m wind anomalies in the region of 20°S–30°N and 175°E–95°W. Similarly, the SPMM is obtained as MCA1 of the cross-covariance matrix between SST and 10-m wind anomalies in this region (35°–10°S and 180°–70°W).

b. Experimental design

To verify the impact of the equatorial western-central Pacific SST anomalies on the winter NPO variability, a set of numerical experiments are conducted based on the Geophysical Fluid Dynamics Laboratory (GFDL) Atmospheric Model version 2.1 (AM2.1) (The GFDL Global Atmospheric Model Development Team 2004). The AM2.1 model features a finite-volume dynamical core with a horizontal resolution of $2.5^{\circ} \times 2.5^{\circ}$ and a vertical resolution composed of 24 levels. This model includes a new gridpoint dynamical core, a prognostic cloud scheme, and a multispecies aerosol climatology, in addition to components inherited from previous GFDL models. We first examined whether the GFDL Coupled Model version 2.1 (CM2.1), which incorporates this atmospheric model component, can reproduce the observed NPO-ENSO relationship. Historical simulations are conducted based on the GFDL CM2.1 model, involving five ensemble members with perturbed initial conditions for temperature T. It shows that this coupled model well reproduces the observed NPO spatial

TABLE 1. Correlation coefficients among used winter NPO index and three winter NPO indices defined based on the EOF method.

	NPO	YK11	PYK13
YK11	0.83		
PYK13	0.80	0.97	
LN08	0.70	0.91	0.91

pattern and the relationship between winter NPO and the following ENSO events with a small ensemble spread (see Fig. S4).

Therefore, we further verify the role of the equatorial westerncentral Pacific SST anomalies in the winter NPO variability based on GFDL AM2.1 by imposing the observed SST anomalies on the climatological annual cycle of SSTs in the tropical westerncentral Pacific region (20°S–20°N, 120°E–160°W). This set of experiments consists of an ensemble of 10 simulations with perturbed initial conditions for temperature T, which are integrated from January 1979 to December 2019. The ensemble mean is used to remove the possible influence of internal atmospheric variability. In our numerical experiments, the perturbations follow a normal distribution with a zero mean and a prescribed standard deviation σ . To be more precise, the perturbations for temperature (T') are specified as $T' = T + \sigma N$, where σ is set to 0.1 K and N represents the standard normal distribution.

3. The observed preceding winter SLP signal over the North Pacific for ENSO

We first revisit the observed lead-lag relationship between ENSO and the SLP anomalies over the North Pacific by regressing

SLP anomalies in the preceding, simultaneous, and subsequent winter on the winter Niño-3.4 index (Fig. 1). The regressed SLP anomaly in the preceding winter exhibits a north-south dipole structure over the North Pacific (Fig. 1a), resembling a typical NPO structure (Walker and Bliss 1932; Rogers 1981). In the simultaneous winter, it is characterized by the negative phase of Southern Oscillation over the tropical Pacific and the enhanced Aleutian low over the extratropical North Pacific (Fig. 1b), manifesting as a traditional ENSO-forced atmospheric teleconnection pattern (e.g., Hoskins and Karoly 1981; Horel and Wallace 1981; Trenberth et al. 1998). In contrast, there are almost no significant SLP anomalies detected in the subsequent winter (Fig. 1c). Here, the NPO index is used to measure the variability of the preexisting winter SLP signal over the North Pacific for ENSO years in Fig. 1a. It is found that the used NPO index in this study is highly consistent with the NPO indices (YK11, PYK13, and LN08) defined based on the EOF method (Fig. 1d, Table 1), and their related SLP patterns are also very similar (Fig. S5).

To further examine the possible linkage of the winter NPO with the ENSO in the following winter, we display SST anomalies in the subsequent winter regressed upon the winter NPO index (Fig. 2a). It shows that a positive NPO event tends to be followed by El Niño–like SST anomalies during the winter of the subsequent year, while a negative NPO event is related to La Niña–like SST anomalies. This leading relationship of NPO over ENSO is also supported by the scatterplot presented in Fig. 2b (r = 0.51, statistically significant at the 95% confidence level). However, it is important to note that not every NPO event is necessarily

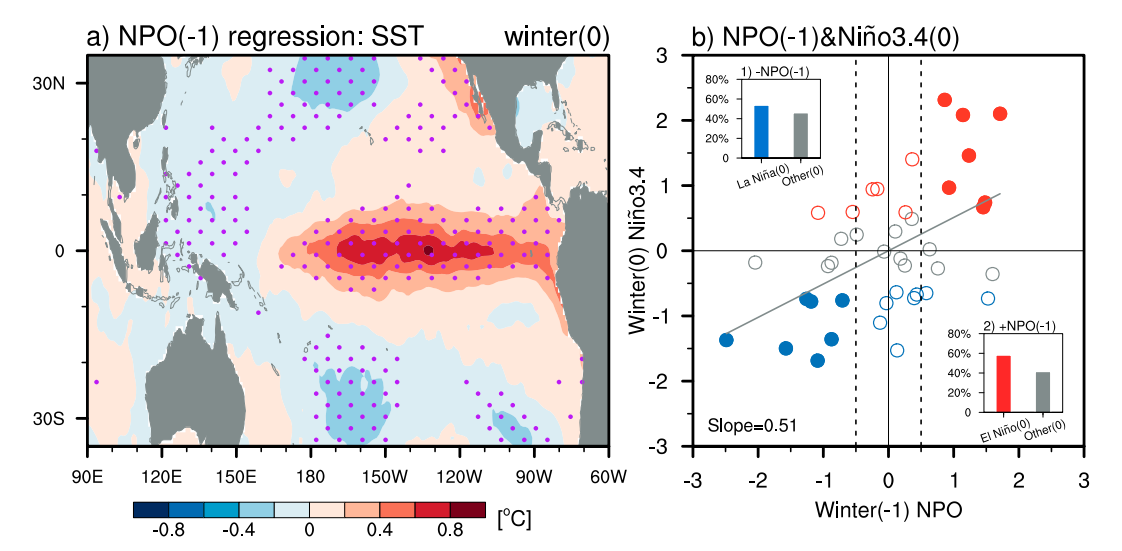


FIG. 2. (a) Regression of SST anomalies (shading; °C) in the subsequent winter upon the winter NPO index. Purple dots indicate regression coefficients that are statistically significant at the 95% confidence level. (b) Scatterplot of normalized winter(-1) NPO against the winter(0) Niño-3.4 index. Red, blue, and gray circles (including solid and hollow circles) denote El Niño, La Niña, and normal years, respectively. El Niño years with a positive NPO phase in the preceding winter are represented by the red solid circles and La Niña years with a negative NPO phase in the preceding winter are represented by the blue solid circles. The linear fit (gray line) is displayed with its slope. Inset 1 shows the occurrence probabilities of La Niña events and other events in the subsequent winter for negative NPO winters. Inset 2 shows the occurrence probabilities of El Niño events and other events in the subsequent winter for positive NPO winters.

TABLE 2. El Niño and La Niña years classified based on the previous winter NPO phase.

El Niño/+NPO	La Niña/-NPO	El Niño/no-NPO	La Niña/no-NPO
1982/83, 1986/87, 1991/92,	1983/84, 1988/89, 1998/99,	1987/88, 1994/95, 2002/03,	1984/85, 1985/86, 1995/96,
1997/98, 2014/15, 2015/16,	1999/2000, 2000/01, 2008/09,	2006/07, 2009/10, 2019/20	2005/06, 2007/08, 2011/12,
2018/19	2010/11		2017/18, 2020/21

followed by an ENSO event in the subsequent winter. As shown in Fig. 2b, approximately 60% of positive NPO events correspond to the following El Niño events, and a similar percentage of negative NPO events is followed by subsequent La Niña events (Fig. 2b). We further categorize these ENSO events into two groups based on their different preceding NPO anomalies (Table 2). The first group is the El Niño years with a previous winter positive NPO phase (El Niño/+NPO) and La Niña years with a previous winter negative NPO phase (La Niña/-NPO). These ENSO events mainly contribute to the statistically positive correlation of winter NPO with the following winter Niño-3.4

indices. The second group consists of the remaining ENSO years, which include El Niño years without a previous winter positive NPO phase (El Niño/no-NPO) and La Niña years without a previous winter negative NPO phase (La Niña/no-NPO).

4. Tropical origin of preceding winter NPO signal for ENSO events

Figures 3a and 3b display the composite differences of the preceding winter SLP, SST, and surface horizontal wind anomalies between El Niño/+NPO and La Niña/-NPO years (i.e., the first

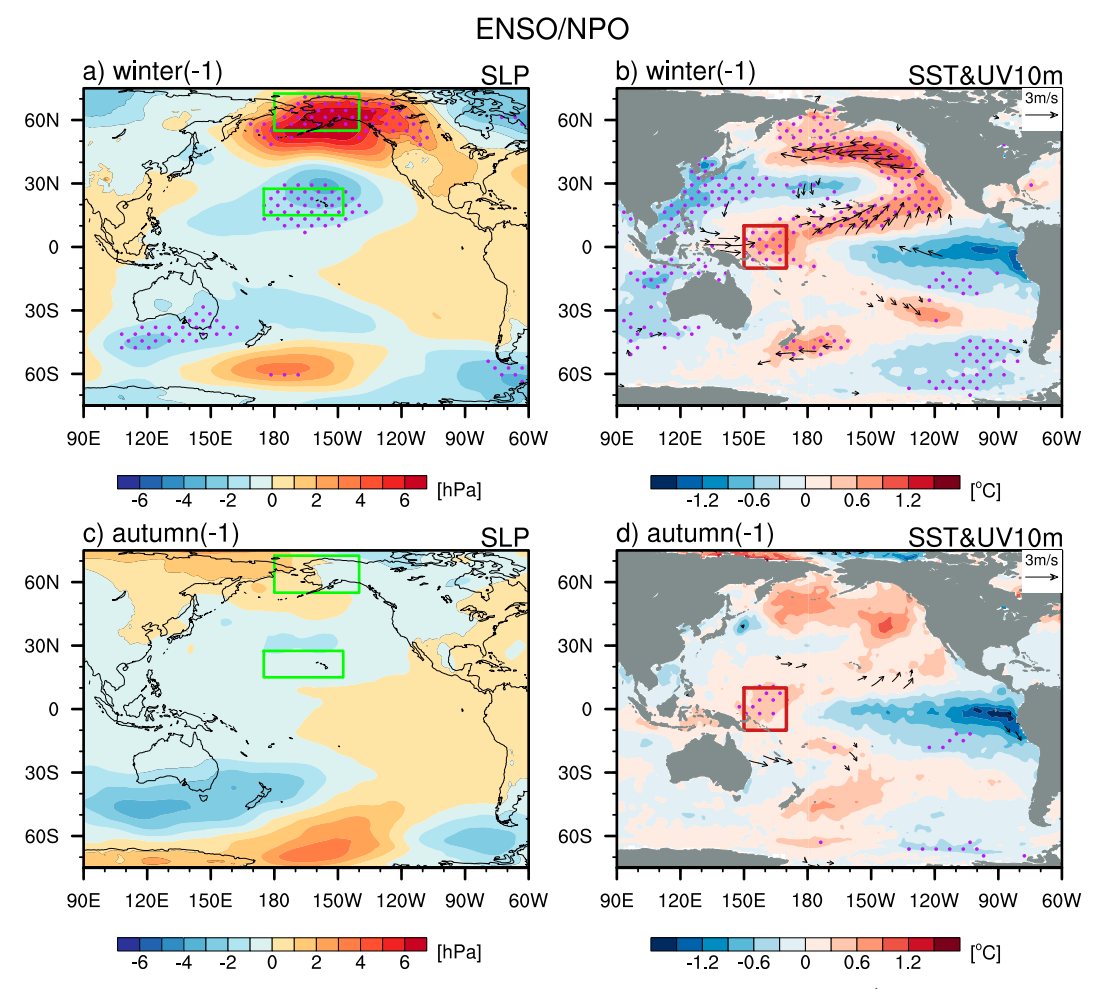


FIG. 3. Composite differences of (a) SLP (hPa) and (b) SST (°C) and horizontal wind (m s⁻¹) anomalies at 10 m in the preceding winter between El Niño/+NPO and La Niña/-NPO years. Purple dots indicate composite values that exceed the 95% significance level. The wind anomalies are shown only when they are significant at the 95% confidence level. (c) As in (a), but in the preceding autumn. (d) As in (b), but in the preceding autumn. The green boxes in (a) and (c) denote the region used to define the NPO index. The red box in (b) and (d) is utilized to define WPI.

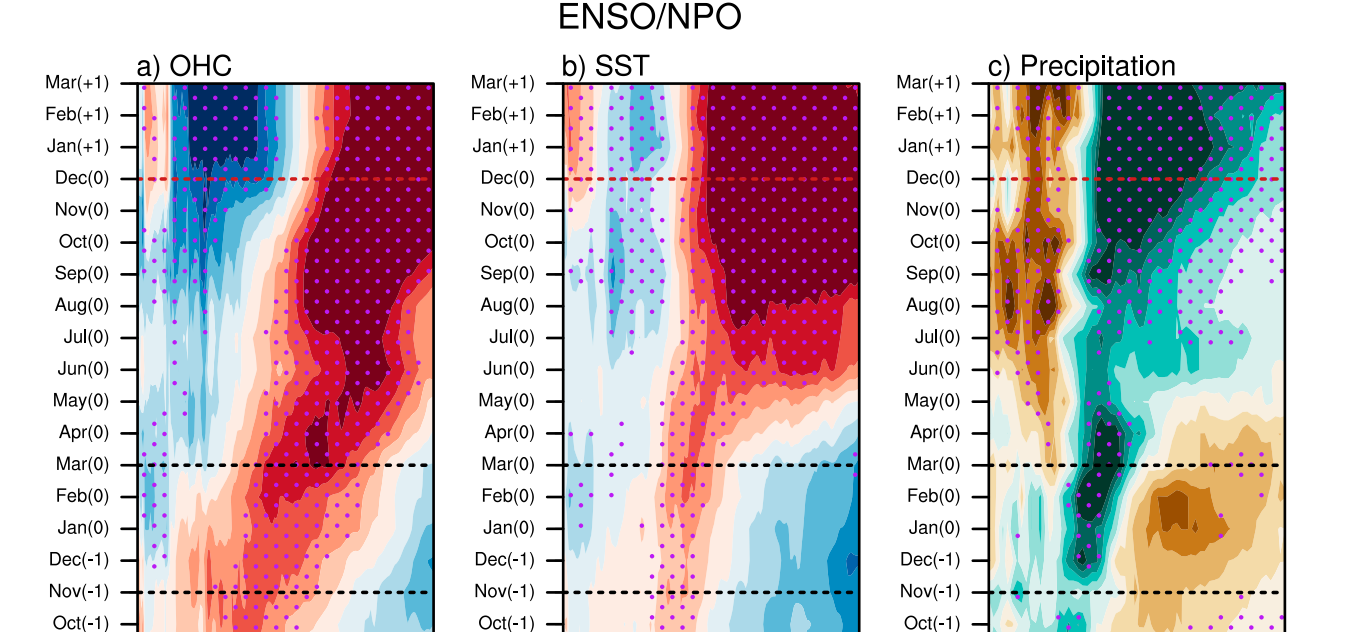


FIG. 4. Time-longitude cross section of anomalous (a) OHC (0–350 m; $^{\circ}$ C), (b) SST ($^{\circ}$ C), and (c) precipitation (mm day $^{-1}$) averaged within 5 $^{\circ}$ S–5 $^{\circ}$ N for the composite difference between El Niño/+NPO and La Niña/-NPO years. Purple dots represent composite values above the 95 $^{\circ}$ C confidence level. The two black dashed lines are used to mark the NPO winter [Nov(-1)-Mar(0)]. The red dashed line denotes the ENSO peak [Dec(0)].

180

-1.2 -0.6 0 0.6 1.2

135E

Sep(-1)

Aug(-1)

Jul(-1)

Jun(-1)

group). The SLP anomalies exhibit a positive NPO spatial pattern over the North Pacific (Fig. 3a). As demonstrated in previous studies (Vimont et al. 2001, 2003b), NPO-related surface wind anomalies could generate a significant tripole SST anomaly pattern over the North Pacific by altering the net surface heat flux, with positive SST anomalies in the midlatitude North Pacific along 40°-60°N, negative SST anomalies in the western-central North Pacific along 20°-40°N, and positive SST anomalies in the subtropical North Pacific (Fig. 3b). This SST anomaly pattern in the North Pacific is very similar to a positive NPMM pattern shown in Fig. S6a, consistent with previous studies suggesting that extratropical NPO signals can induce SST anomalies resembling the NPMM pattern (Chiang and Vimont 2004; Stuecker 2018). Simultaneously, there are some significant SST and wind anomalies in the subtropical South Pacific, while the spatial pattern is different from the SPMM pattern in Fig. S6b. It is worth noting that there are significantly positive SST anomalies and corresponding surface westerly wind anomalies observed in the equatorial western-central Pacific during the winter period coinciding with the NPO signal. These anomalies also have the potential to trigger circulation anomalies associated with the NPO by stimulating convection anomaly patterns. We further examine the composite differences of SLP, SST, and surface horizontal wind anomalies in

135W

Sep(-1)

Aug(-1)

Jul(-1)

Jun(-1)

135E

-1.2 -0.6 0

180

0.6 1.2

the preceding autumn prior to winter NPO signal for this group of ENSO years (Figs. 3c,d). It is intriguing to note that the presence of local warm SST anomalies in the equatorial westerncentral Pacific can be observed one season ahead, while significant atmospheric circulation anomalies are absent over the North Pacific. In the preceding autumn, there are almost no NPMM or SPMM patterns observed over the subtropical North and South Pacific. The asynchronous nature of the SST anomalies and the associated circulation patterns adds to the complexity of the phenomenon and calls for detailed investigation.

Sep(-1) Aug(-1)

Jul(-1)

Jun(-1)

135E

180

135W

135W

[mm/day]

Figure 4a shows the time evolution of the OHC anomalies for the first group based on their composite difference between El Niño/+NPO and La Niña/-NPO years. During the preceding summer and autumn before the winter NPO signal, there exist significantly positive OHC anomalies in the equatorial western and central Pacific, corresponding to local warm SST anomalies in this region (Fig. 4b). These positive anomalies in OHC and SST gradually evolve in the subsequent seasons. This development is accompanied by positive precipitation anomalies that are coupled with the local warm SST anomalies in the same region (Fig. 4c). In the following spring and summer, these OHC and SST anomalies migrate eastward toward the equatorial central-eastern Pacific and

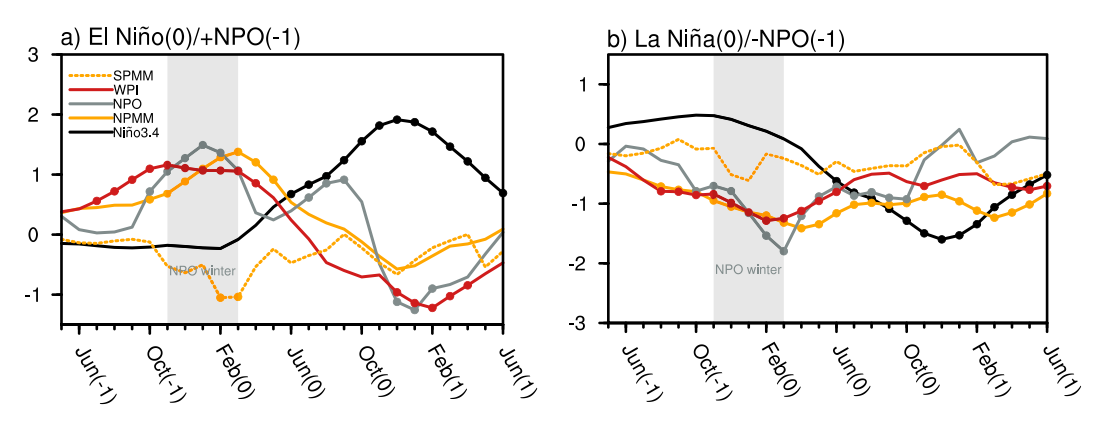


FIG. 5. Composite time evolution of normalized monthly WPI (red line), NPO index (gray line), Niño-3.4 index (black line), NPMM index (orange solid line), and SPMM index (orange dashed line) for the (a) El Niño/+NPO and (b) La Niña/-NPO years. The solid dots denote anomalies that are statistically significant at the 95% confidence level. The abscissa indicates 26 months from May of the year(-1) to June of the year(1). The gray shading area represents the NPO winter.

develop into an El Niño event in the following autumn and winter, accompanied by typical ENSO-associated dipole precipitation anomalies. The observational analyses provide evidence of the existence of precursory ocean–atmosphere signals in the tropical Pacific prior to the winter NPO signal.

5. The role of equatorial western-central SST anomalies in the winter NPO

Building on the above leading relationship, we propose a hypothesis that the preceding winter NPO signal for ENSO events may be influenced by equatorial western-central SST anomalies. To investigate the role of tropical Pacific SST anomalies in the preceding winter NPO, we introduce the WPI as a metric for measuring SST variability in the equatorial western-central region (10°S-10°N, 150°-170°E). The temporal evolution of WPI, NPO, and Niño-3.4, NPMM, and SPMM indices for the ENSO years with the preceding winter NPO is depicted in Fig. 5. During both these El Niño and La Niña years, we consistently observe significant NPO anomalies throughout the preceding winter, starting from October of the previous year [Oct(-1)]. NPMM closely follows the evolution of NPO, with a lag of 1-2 months. This aligns with previous studies suggesting that the NPO could initiate the NPMM. In contrast, almost no significant SPMM signal is observed in the development process of ENSO/NPO events. Notably, the significant WPI anomalies appear as early as July of the previous year [Jul(-1)] and persist into the subsequent autumn and winter. The different timing of significant anomalies in NPO and WPI warrants a cautious examination of their causal relationship. Figure 6a displays the time series of winter NPO and WPI. It shows that they vary in a similar manner, displaying a substantial correlation coefficient of 0.69 (statistically above the 95% confidence level). Correspondingly, the WPI-associated SLP anomalies exhibit a north-south dipole pattern over the North Pacific (Fig. 7b), which highly resembles those related to the NPO (Fig. 7a). To further identify

their causal relationship, we display in Figs. 6b and 6c the autumn and winter WPI for those ENSO years contributing to the statistically positive correlation of winter NPI with the following winter Niño-3.4 index (i.e., the first group of ENSO years). For all the El Niño/+NPO events, the previous winter WPI exhibits a positive anomaly, which can be traced to the preceding autumn (Fig. 6b). Conversely, for La Niña/-NPO years, the WPI largely displays a negative anomaly during both previous autumn and winter seasons (Fig. 6c). It shows that the winter local SST signal for these ENSO years can be detected during the preceding autumn, prior to the winter NPO signal, suggesting that the preceding winter NPO signal of ENSO events could be largely attributed to the anomalies in the local tropical Pacific SST. It is found that winter WPI has a positive correlation with the following winter Niño-3.4 index (R = 0.45), which is comparable to the correlation between winter NPO and the following winter Niño-3.4 index (R = 0.51). The statistical relationship between NPO and the following winter ENSO could be largely explained by the western-central tropical Pacific SST signal.

In Fig. 8, we also investigate the composite differences in the ocean-atmosphere conditions during the preceding winter and autumn between El Niño/no-NPO and La Niña/no-NPO years (i.e., the second group). Similarly, no significant oceanic and atmospheric precursors can be observed in the tropical Pacific during the simultaneous period (i.e., the preceding autumn and winter of ENSO years) (Fig. 9), distinctly different from the first group of ENSO events. Interestingly, remarkable OHC and SST anomalies appear in the tropical central and eastern Pacific during the developing summer of ENSO events rather than the earlier seasons and reach their peak in the following winter, accompanied by dipole precipitation anomalies. Upon the comparison between the two groups of ENSO events, the occurrence of the NPO signal preceding ENSO could potentially serve as a companion to ENSO development. This companionship is established through the

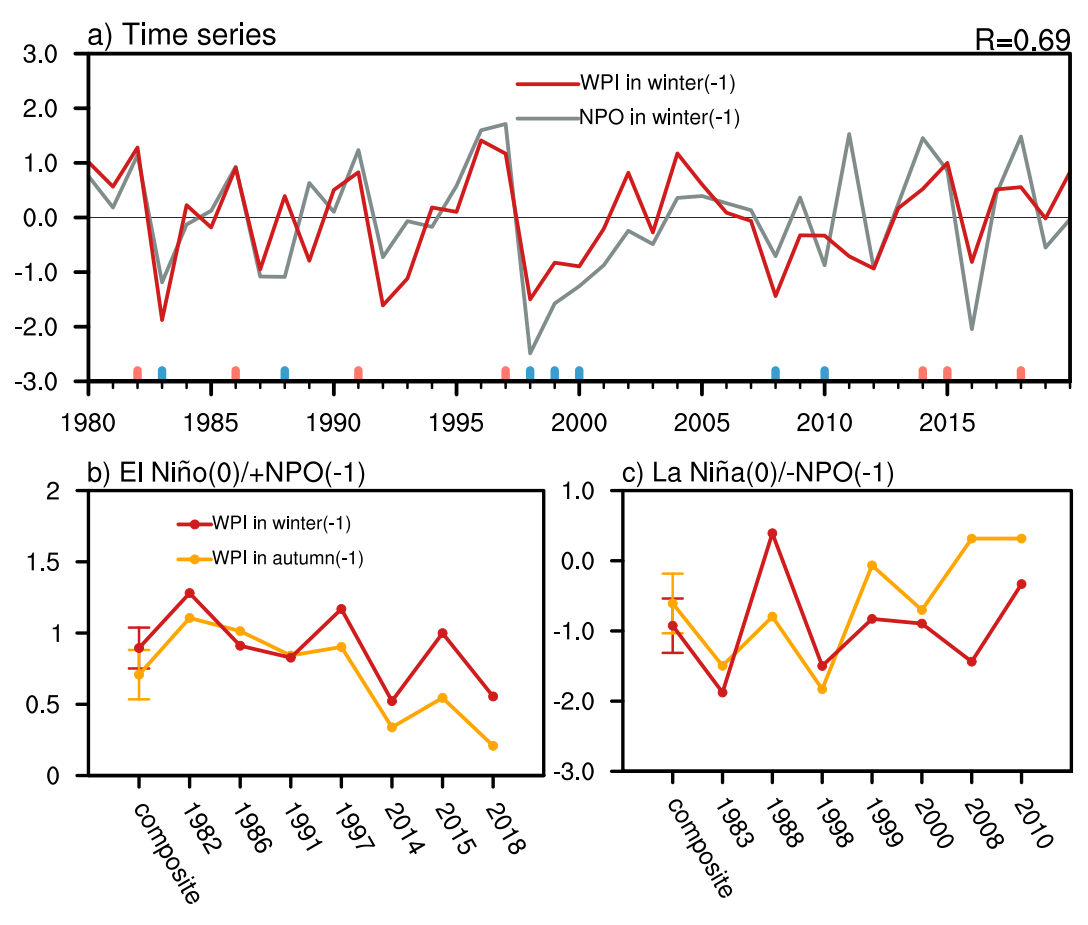


FIG. 6. (a) Normalized time series of the winter NPO (gray line) and WPI (red line). The El Niño/+NPO and La Niña/-NPO years are marked by red and blue vertical lines, respectively. (b) The autumn (orange dotted line) and winter (red dotted line) WPI for El Niño/+NPO events. The first dot is the composite value for these years and the error bars denote one standard deviation error estimate. (c) As in (b), but for La Niña/-NPO events.

presence of preexisting SST anomalies in the equatorial western-central Pacific region.

To further verify the influence of the tropical Pacific SST anomalies on the NPO, a set of atmospheric general circulation model (AGCM) experiments is conducted (refer to

experimental designs in section 2) by imposing the observed monthly SST anomalies in the tropical western–central Pacific (Fig. 10a). Remarkably, the AGCM simulations generally reproduce the observed SLP anomaly pattern associated with the WPI. However, there is a slight rotation in the centers of

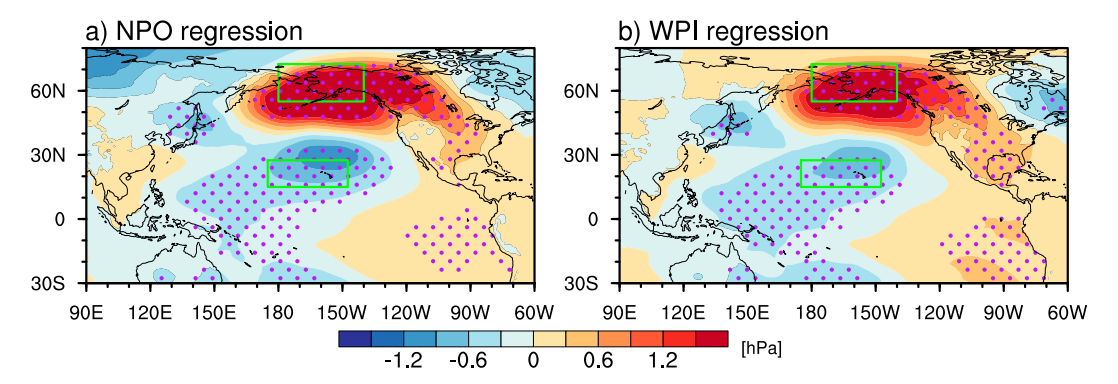


FIG. 7. Regression of SLP anomalies (shading; hPa) upon the winter (a) NPO and (b) WPI. Purple dots indicate regression coefficients that are statistically significant at the 95% confidence level. The green boxes in (a) and (b) denote the region used to define NPO.

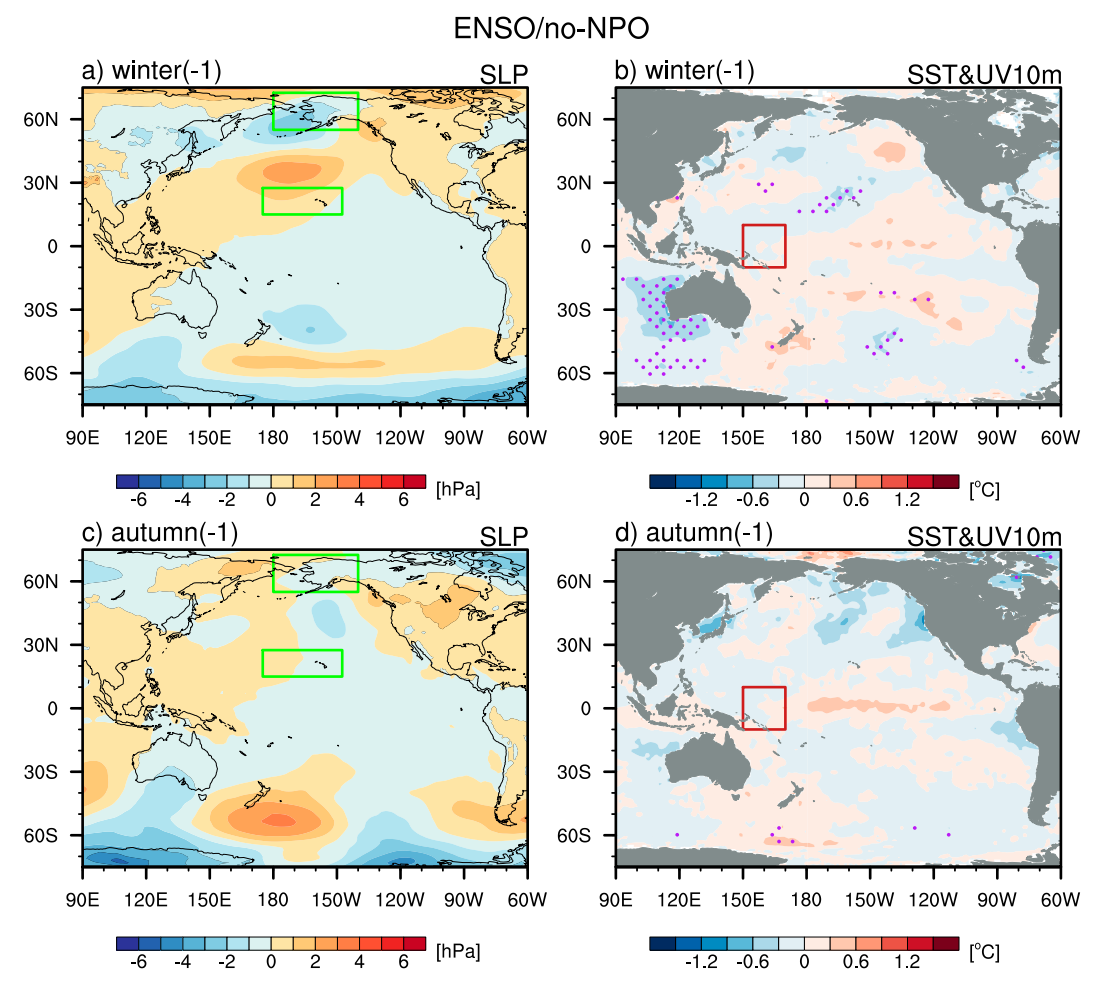


FIG. 8. Composite differences of (a) SLP (hPa) and (b) SST (°C) and horizontal wind (m s⁻¹) anomalies at 10 m in the preceding winter between El Niño/no-NPO and La Niña/no-NPO years. Purple dots indicate composite values that exceed the 95% significance level. The wind anomalies are shown only when they are significant at the 95% confidence level. (c) As in (a), but in the preceding autumn. (d) As in (b), but in the preceding autumn. The green boxes in (a) and (c) denote the region used to define NPO. The red box in (b) and (d) is utilized to define WPI.

action relative to the observations, and the amplitude of SLP anomalies in the simulations is relatively weaker than that observed (Figs. 7b and 10b). This discrepancy is possibly related to the model bias such as the representation of the tropical Pacific mean state. Across the North Pacific, a notable positive SLP anomaly center emerges in Alaska and a lowpressure anomaly center is near Hawaii, exhibiting a northsouth dipole spatial structure akin to the NPO pattern. As shown in Fig. 10c, the simulated NPO has a high correlation with the observed NPO (r = 0.74, statistically significant at 99% confidence level), suggesting that the equatorial western and central Pacific SST anomalies significantly contribute to the variability of the NPO during the period of 1979-2021. Consequently, it was possible to establish a positive relationship between the simulated winter NPO, forced by tropical Pacific SST anomalies, and the following winter Niño-3.4 index (r = 0.49, statistically significant at the 99% confidence level). These modeling results provide further evidence that the preceding winter NPO signal is largely a result of SST forcing in the equatorial central-western Pacific. This result is consistent with a previous finding of Wu et al. (2019), where they identified a close linkage between the NPO-related atmospheric circulation anomalies and a tropical zonal dipole SST pattern, which includes the western-central equatorial Pacific SST anomalies imposed in our experiments.

6. Conclusions and discussion

The present study aims to enhance our understanding of the preceding atmospheric signal over the North Pacific for ENSO events based on comprehensive analyses of observations and targeted experiments using an atmospheric general circulation model. The NPO-like SLP anomalies are observed over the North Pacific in the preceding winter of approximately 60% of the ENSO years observed in the period of 1979–2021. Our

ENSO/no NPO

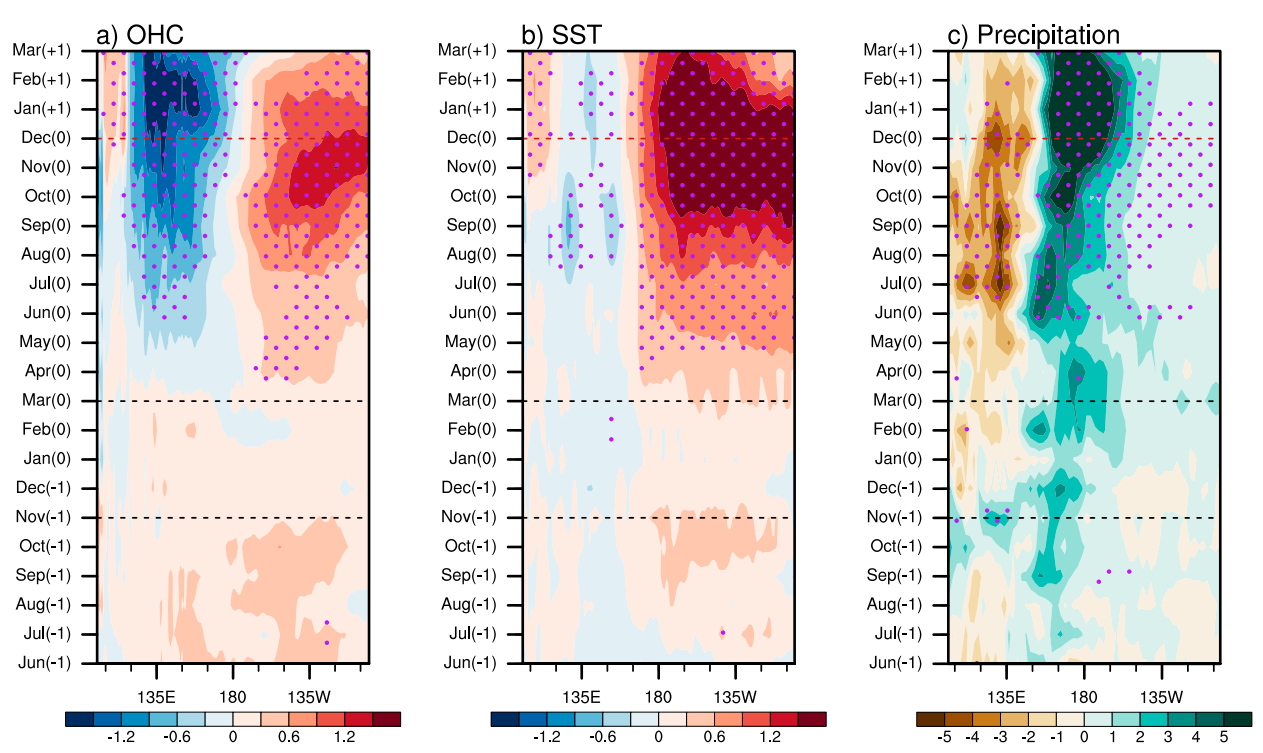


FIG. 9. Time-longitude cross section of anomalous (a) OHC (0–350 m; $^{\circ}$ C), (b) SST ($^{\circ}$ C), and (c) precipitation (mm day $^{-1}$) averaged within 5 $^{\circ}$ S–5 $^{\circ}$ N for the composite difference between El Niño/no-NPO and La Niña/no-NPO years. Purple dots represent composite values above the 95 $^{\circ}$ C confidence level. The two black dashed lines are used to mark the NPO winter [Nov(-1)–Mar(0)]. The red dashed line denotes the ENSO peak [Dec(0)].

study demonstrates that this preexisting winter NPO signal primarily originates from the equatorial western-central Pacific SST forcing. The ENSO years with a preceding winter NPO signal are characterized by significant SST anomalies in the tropical central and western Pacific during the preceding autumn and winter. These local SST anomalies play a crucial role in driving an atmospheric circulation anomaly similar to the NPO pattern by stimulating convection anomalies. Modeling experiments conducted in our study provide further evidence supporting the argument that the SST anomalies in the equatorial western-central Pacific could drive the NPO-like circulation pattern. For the remaining ENSO years, no remarkable SST anomalies are observed in the equatorial western-central Pacific during the preceding winter. Consequently, there is also a lack of a preceding NPO signal in these ENSO years.

This work highlights the crucial role of air-sea anomalies in the deep tropics in triggering the preceding winter NPO signal of ENSO events. However, the source of the preexisting western-central SST signal for ENSO events remains unresolved. The previous winter local SST signal in the equatorial western-central Pacific for some ENSO/NPO events (e.g., 1986, 1997, 1998, and 2018) is accompanied by opposite-sign SST anomalies in the equatorial eastern Pacific (not shown), implying its potential association with

the cyclic ENSO transition. Some studies also show that the first year of some multiyear ENSO events corresponds to this local SST anomaly, suggesting a possible link to the multiyear ENSO events (Park et al. 2021; Fang and Yu 2020; Wu et al. 2019). Certain high-frequency atmospheric signals in the tropical Pacific, such as westerly wind events (WWEs) (McPhaden et al. 1992; McPhaden 1999) and Madden–Julian oscillation (Madden and Julian 1994), may also contribute to the appearance of this local SST signal. In addition, South Pacific Ocean variability could also play a role (Dong et al. 2022; You and Furtado 2018). Further research is necessary to identify the precise sources of the SST signal on an event-by-event basis.

It is important to note that our findings do not dismiss the possibility that the NPO may, in turn, exert some physical feedback on the tropical Pacific by mechanisms including SFM, TWC, and upper-tropospheric wave propagation (Vimont et al. 2001; Anderson et al. 2013; Zhao et al. 2023a). Our present work suggests that the lagged relationship between ENSO and the NPO represents a tropical–extratropical two-way coupling rather than a stochastic forcing of the extratropical atmosphere on ENSO. To better understand this coupling, future investigations should aim to quantify the feedback from NPO to subsequent ENSO events by decoupling the tropics and extratropics in a coupled model.

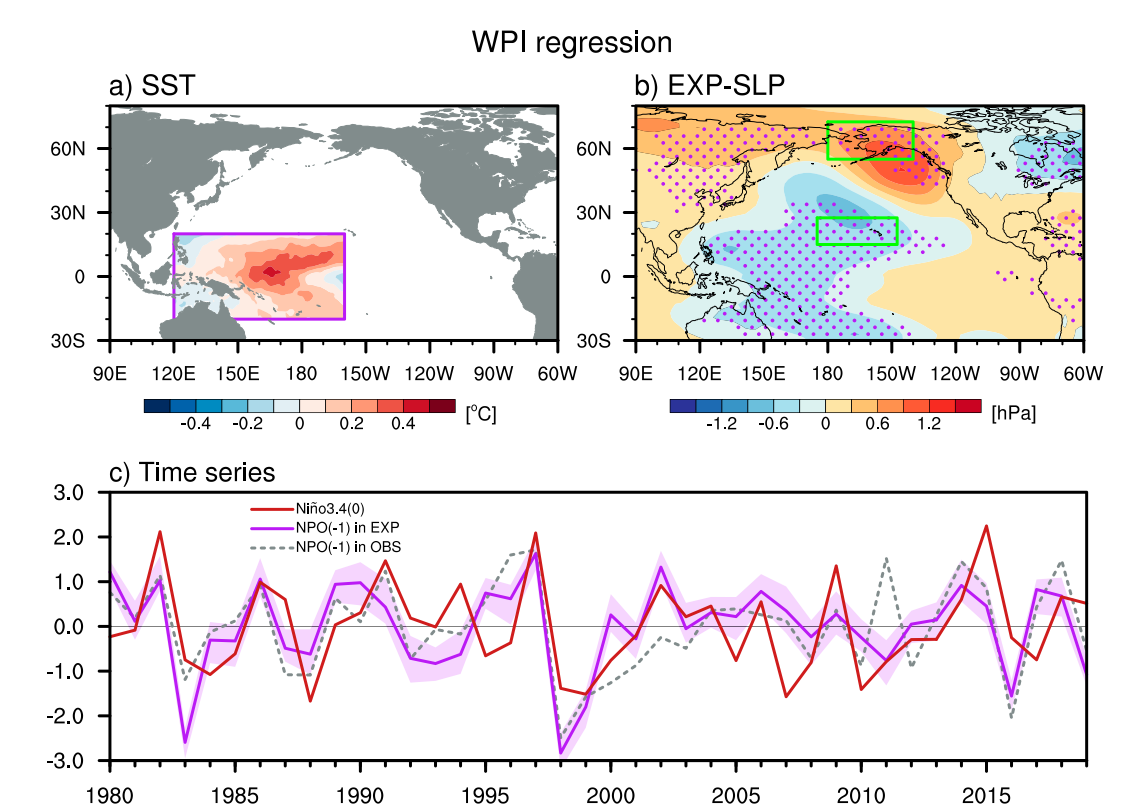


FIG. 10. (a) Regression of SST anomalies (shading; °C) upon the winter WPI. The purple box is used to denote the SST forcing region in the numerical experiments. The values that are not in this region are not shown. (b) Regression of simulated (shading; hPa) SLP anomalies upon the winter WPI. Purple dots indicate regression coefficients that are statistically significant at the 95% confidence level. (c) Normalized time series of the winter Niño-3.4 index (red solid line), NPO in the experiment (purple solid line), and NPO in the observation (gray dashed line). The purple shading represents the ensemble spread.

Acknowledgments. We thank Jong-Seong Kug for useful comments on the early version of this work. This work is supported by the National Nature Science Foundation of China (42088101). M. W. is supported by the Program for Advanced Studies of Climate Change Projection (SENTAN) Grantin-Aid JPMXD0722680395 from the Ministry of Education, Culture, Sports, Science, and Technology (MEXT), Japan. S. H. is supported by the Postgraduate Research and Practice Innovation Program of Jiangsu Province (KYCX22_1132).

Data availability statement. The data that support the findings of this study are available from the following resources: ERA5 dataset can be obtained from https://cds.climate.copernicus.eu/cdsapp#!/dataset/reanalysis-era5-single-levelsmonthly-means?tab=form; HadISST data are available at https://www.metoffice.gov.uk/hadobs/hadisst/data/download.html; Monthly subsurface ocean temperature data are from https://cds.climate.copernicus.eu/cdsapp#!/dataset/reanalysis-oras5?tab=overview; CMAP precipitation data are derived from https://psl.noaa.gov/data/gridded/data.cmap.html.

REFERENCES

Alexander, M. A., I. Bladé, M. Newman, J. R. Lanzante, N.-C. Lau, and J. D. Scott, 2002: The atmospheric bridge: The influence of ENSO teleconnections on air–sea interaction over the global oceans. *J. Climate*, **15**, 2205–2231, https://doi.org/10.1175/1520-0442(2002)015<2205:TABTIO>2.0.CO;2.

Amaya, D. J., Y. Kosaka, W. Zhou, Y. Zhang, S.-P. Xie, and A. J. Miller, 2019: The North Pacific pacemaker effect on historical ENSO and its mechanisms. *J. Climate*, 32, 7643–7661, https://doi.org/10.1175/JCLI-D-19-0040.1.

Anderson, B. T., 2003: Tropical Pacific sea-surface temperatures and preceding sea level pressure anomalies in the subtropical North Pacific. J. Geophys. Res., 108, 4732, https://doi.org/10. 1029/2003JD003805.

—, 2004: Investigation of a large-scale mode of ocean–atmosphere variability and its relation to tropical Pacific sea surface temperature anomalies. J. Climate, 17, 4089–4098, https://doi.org/10.1175/ 1520-0442(2004)017<4089:IOALMO>2.0.CO;2.

—, 2007: On the joint role of subtropical atmospheric variability and equatorial subsurface heat content anomalies in initiating the onset of ENSO events. *J. Climate*, 20, 1593–1599, https:// doi.org/10.1175/JCLI4075.1.

——, R. C. Perez, and A. Karspeck, 2013: Triggering of El Niño onset through trade wind-induced charging of the equatorial Pacific. *Geophys. Res. Lett.*, 40, 1212–1216, https://doi.org/10.1002/grl.50200.

Ashok, K., C.-Y. Tam, and W.-J. Lee, 2009: ENSO Modoki impact on the Southern Hemisphere storm track activity during extended austral winter. *Geophys. Res. Lett.*, 36, L12705, https://doi.org/10.1029/2009GL038847.

- Bayr, T., D. I. V. Domeisen, and C. Wengel, 2019: The effect of the equatorial Pacific cold SST bias on simulated ENSO teleconnections to the North Pacific and California. *Climate Dyn.*, 53, 3771– 3789, https://doi.org/10.1007/s00382-019-04746-9.
- Bjerknes, J., 1969: Atmospheric teleconnections from the equatorial Pacific. *Mon. Wea. Rev.*, **97**, 163–172, https://doi.org/10. 1175/1520-0493(1969)097<0163:ATFTEP>2.3.CO;2.
- Bosc, C., and T. Delcroix, 2008: Observed equatorial Rossby waves and ENSO-related warm water volume changes in the equatorial Pacific Ocean. J. Geophys. Res., 113, C06003, https://doi.org/10. 1029/2007JC004613.
- Bunge, L., and A. J. Clarke, 2014: On the warm water volume and its changing relationship with ENSO. J. Phys. Oceanogr., 44, 1372–1385, https://doi.org/10.1175/JPO-D-13-062.1.
- Cane, M. A., and S. E. Zebiak, 1985: A theory for El Niño and the Southern Oscillation. *Science*, 228, 1085–1087, https://doi. org/10.1126/science.228.4703.1085.
- Chang, P., L. Zhang, R. Saravanan, D. J. Vimont, J. C. H. Chiang, L. Ji, H. Seidel, and M. K. Tippett, 2007: Pacific meridional mode and El Niño–Southern Oscillation. *Geophys. Res. Lett.*, 34, L16608, https://doi.org/10.1029/2007GL030302.
- Chen, H.-C., Y.-H. Tseng, Z.-Z. Hu, and R. Ding, 2020: Enhancing the ENSO predictability beyond the spring barrier. *Sci. Rep.*, **10**, 984, https://doi.org/10.1038/s41598-020-57853-7.
- Chiang, J. C. H., and D. J. Vimont, 2004: Analogous Pacific and Atlantic meridional modes of tropical atmosphere–ocean variability. *J. Climate*, 17, 4143–4158, https://doi.org/10.1175/ JCLI4953.1.
- Davis, R. E., 1976: Predictability of sea surface temperature and sea level pressure anomalies over the North Pacific Ocean. *J. Phys. Oceanogr.*, **6**, 249–266, https://doi.org/10.1175/1520-0485(1976)006 <0249:POSSTA>2.0.CO;2.
- Deser, C., and Coauthors, 2012: ENSO and Pacific decadal variability in the Community Climate System Model version 4. *J. Climate*, **25**, 2622–2651, https://doi.org/10.1175/JCLI-D-11-00301.1.
- Di Lorenzo, E., K. M. Cobb, J. C. Furtado, N. Schneider, B. T. Anderson, A. Bracco, M. A. Alexander, and D. J. Vimont, 2010: Central Pacific El Niño and decadal climate change in the North Pacific Ocean. *Nat. Geosci.*, 3, 762–765, https://doi.org/10.1038/ngeo984.
- Ding, R., and Coauthors, 2022: Multi-year El Niño events tied to the North Pacific Oscillation. *Nat. Commun.*, 13, 3871, https://doi.org/10.1038/s41467-022-31516-9.
- Dong, Y., K. C. Armour, D. S. Battisti, and E. Blanchard-Wrigglesworth, 2022: Two-way teleconnections between the Southern Ocean and the tropical Pacific via a dynamic feedback. J. Climate, 35, 6267–6282, https://doi.org/10.1175/JCLI-D-22-0080.1.
- Fang, S.-W., and J.-Y. Yu, 2020: A control of ENSO transition complexity by tropical Pacific mean SSTs through tropical-subtropical interaction. *Geophys. Res. Lett.*, 47, e2020GL087933, https://doi.org/10.1029/2020GL087933.
- Furtado, J. C., E. Di Lorenzo, B. T. Anderson, and N. Schneider, 2012: Linkages between the North Pacific Oscillation and central tropical Pacific SSTs at low frequencies. Climate Dyn., 39, 2833–2846, https://doi.org/10.1007/s00382-011-1245-4.
- Guo, Y., M. Ting, Z. Wen, and D. E. Lee, 2017: Distinct patterns of tropical Pacific SST anomaly and their impacts on North

- American climate. *J. Climate*, **30**, 5221–5241, https://doi.org/10.1175/JCLI-D-16-0488.1.
- Hendon, H. H., E. Lim, G. Wang, O. Alves, and D. Hudson, 2009: Prospects for predicting two flavors of El Niño. Geophys. Res. Lett., 36, L19713, https://doi.org/10.1029/2009 GL040100.
- Hersbach, H., and Coauthors, 2020: The ERA5 global reanalysis. *Quart. J. Roy. Meteor. Soc.*, **146**, 1999–2049, https://doi.org/10.1002/qj.3803.
- Hoell, A., M. Hoerling, J. Eischeid, K. Wolter, R. Dole, J. Perlwitz, T. Xu, and L. Cheng, 2016: Does El Niño intensity matter for California precipitation? *Geophys. Res. Lett.*, 43, 819–825, https://doi.org/10.1002/2015GL067102.
- Horel, J. D., and J. M. Wallace, 1981: Planetary-scale atmospheric phenomena associated with the Southern Oscillation. *Mon. Wea. Rev.*, 109, 813–829, https://doi.org/10.1175/1520-0493(1981)109 <0813:PSAPAW>2.0.CO;2.
- Hoskins, B. J., and D. J. Karoly, 1981: The steady linear response of a spherical atmosphere to thermal and orographic forcing. *J. Atmos. Sci.*, **38**, 1179–1196, https://doi.org/10.1175/1520-0469(1981)038<1179:TSLROA>2.0.CO;2.
- Jin, F.-F., 1997a: An equatorial ocean recharge paradigm for ENSO. Part I: Conceptual model. J. Atmos. Sci., 54, 811–829, https://doi.org/10.1175/1520-0469(1997)054<0811:AEORPF> 2.0.CO:2.
- —, 1997b: An equatorial ocean recharge paradigm for ENSO. Part II: A stripped-down coupled model. *J. Atmos. Sci.*, **54**, 830–847, https://doi.org/10.1175/1520-0469(1997)054<0830: AEORPF>2.0.CO;2.
- Kumar, A., M. Chen, Y. Xue, and D. Behringer, 2015: An analysis of the temporal evolution of ENSO prediction skill in the context of the equatorial Pacific Ocean observing system. Mon. Wea. Rev., 143, 3204–3213, https://doi.org/10.1175/MWR-D-15-0035.1.
- Lau, N.-C., 1997: Interactions between global SST anomalies and the midlatitude atmospheric circulation. *Bull. Amer. Meteor. Soc.*, **78**, 21–34, https://doi.org/10.1175/1520-0477(1997)078 <0021:IBGSAA>2.0.CO;2.
- Linkin, M. E., and S. Nigam, 2008: The North Pacific Oscillation—west Pacific teleconnection pattern: Mature-phase structure and winter impacts. J. Climate, 21, 1979–1997, https://doi.org/10.1175/2007JCLI2048.1.
- Madden, R. A., and P. R. Julian, 1994: Observations of the 40–50-day tropical oscillation—A review. *Mon. Wea. Rev.*, **122**, 814–837, https://doi.org/10.1175/1520-0493(1994)122<0814:OOTDTO> 2.0.CO:2.
- McPhaden, M. J., 1999: Genesis and evolution of the 1997–98 El Niño. Science, 283, 950–954, https://doi.org/10.1126/science. 283.5404.950.
- ——, 2003: Tropical Pacific Ocean heat content variations and ENSO persistence barriers. *Geophys. Res. Lett.*, 30, 1480, https://doi.org/10.1029/2003GL016872.
- ——, 2012: A 21st century shift in the relationship between ENSO SST and warm water volume anomalies. *Geophys. Res. Lett.*, 39, L09706, https://doi.org/10.1029/2012GL051826.
- —, F. Bahr, Y. Du Penhoat, E. Firing, S. P. Hayes, P. P. Niiler, P. L. Richardson, and J. M. Toole, 1992: The response of the western equatorial Pacific Ocean to westerly wind bursts during November 1989 to January 1990. J. Geophys. Res., 97, 14289–14303, https://doi.org/10.1029/92JC01197.
- Meinen, C. S., and M. J. McPhaden, 2000: Observations of warm water volume changes in the equatorial Pacific and their relationship to

- El Niño and La Niña. *J. Climate*, **13**, 3551–3559, https://doi.org/10.1175/1520-0442(2000)013<3551:OOWWVC> 2.0.CO:2.
- Nakamura, T., Y. Tachibana, M. Honda, and S. Yamane, 2006: Influence of the Northern Hemisphere annular mode on ENSO by modulating westerly wind bursts. *Geophys. Res. Lett.*, 33, L07709, https://doi.org/10.1029/ 2005GL025432.
- Neelin, J. D., D. S. Battisti, A. C. Hirst, F.-F. Jin, Y. Wakata, T. Yamagata, and S. E. Zebiak, 1998: ENSO theory. *J. Geophys. Res.*, 103, 14261–14290, https://doi.org/10.1029/97JC03424.
- Park, J.-H., S.-I. An, J.-S. Kug, Y.-M. Yang, T. Li, and H.-S. Jo, 2021: Mid-latitude leading double-dip La Niña. *Int. J. Climatol.*, 41, E1353–E1370, https://doi.org/10.1002/joc.6772.
- Park, J.-Y., S.-W. Yeh, J.-S. Kug, and J. Yoon, 2013: Favorable connections between seasonal footprinting mechanism and El Niño. Climate Dyn., 40, 1169–1181, https://doi.org/10.1007/s00382-012-1477-y.
- Parnell, A. C., 2013: Climate time series analysis: Classical statistical and bootstrap methods. *J. Time Ser. Anal.*, 34, 281–281, https://doi.org/10.1111/jtsa.12002.
- Pegion, K., C. M. Selman, S. Larson, J. C. Furtado, and E. J. Becker, 2020: The impact of the extratropics on ENSO diversity and predictability. *Climate Dyn.*, 54, 4469–4484, https://doi.org/10.1007/s00382-020-05232-3.
- Philander, S. G. H., 1985: El Niño and La Niña. *J. Atmos. Sci.*, **42**, 2652–2662, https://doi.org/10.1175/1520-0469(1985)042<2652: ENALN>2.0.CO;2.
- Rayner, N. A., D. E. Parker, E. B. Horton, C. K. Folland, L. V. Alexander, D. P. Rowell, E. C. Kent, and A. Kaplan, 2003: Global analyses of sea surface temperature, sea ice, and night marine air temperature since the late nineteenth century. J. Geophys. Res., 108, 4407, https://doi.org/10.1029/2002JD 002670.
- Rogers, J. C., 1981: The North Pacific Oscillation. *J. Climatol.*, **1**, 39–57, https://doi.org/10.1002/joc.3370010106.
- Ropelewski, C. F., and M. S. Halpert, 1987: Global and regional scale precipitation patterns associated with the El Niño/Southern Oscillation. *Mon. Wea. Rev.*, 115, 1606–1626, https://doi.org/10.1175/ 1520-0493(1987)115<1606:GARSPP>2.0.CO;2.
- Stuecker, M. F., 2018: Revisiting the Pacific Meridional Mode. *Sci. Rep.*, **8**, 3216, https://doi.org/10.1038/s41598-018-21537-0.
- Terray, P., 2011: Southern Hemisphere extra-tropical forcing: A new paradigm for El Niño-Southern Oscillation. *Climate Dyn.*, **36**, 2171–2199, https://doi.org/10.1007/s00382-010-0825-z.
- The GFDL Global Atmospheric Model Development Team, 2004: The new GFDL Global Atmosphere and Land Model AM2–LM2: Evaluation with prescribed SST simulations. *J. Climate*, 17, 4641–4673, https://doi.org/10.1175/JCLI-3223.1.
- Trascasa-Castro, P., A. C. Maycock, Y. Ruprich-Robert, M. Turco, and P. W. Staten, 2023: Atlantic multidecadal variability modulates the climate impacts of El Niño–Southern Oscillation in Australia. *Environ. Res. Lett.*, 18, 084029, https://doi.org/10.1088/1748-9326/ace920.
- Trenberth, K. E., G. W. Branstator, D. Karoly, A. Kumar, N.-C. Lau, and C. Ropelewski, 1998: Progress during TOGA in understanding and modeling global teleconnections associated with tropical sea surface temperatures. *J. Geophys. Res.*, 103, 14291–14324, https://doi.org/10.1029/97JC01444.
- Tseng, Y., J.-H. Huang, and H.-C. Chen, 2022: Improving the predictability of two types of ENSO by the characteristics of extratropical

- precursors. *Geophys. Res. Lett.*, **49**, e2021GL097190, https://doi.org/10.1029/2021GL097190.
- van Loon, H., and R. A. Madden, 1981: The Southern Oscillation. Part I: Global associations with pressure and temperature in northern winter. *Mon. Wea. Rev.*, 109, 1150–1162, https://doi. org/10.1175/1520-0493(1981)109<1150:TSOPIG>2.0.CO;2.
- Vimont, D. J., D. S. Battisti, and A. C. Hirst, 2001: Footprinting: A seasonal connection between the tropics and mid-latitudes. *Geophys. Res. Lett.*, 28, 3923–3926, https://doi.org/10.1029/ 2001GL013435.
- —, and —, 2003a: The seasonal footprinting mechanism in the CSIRO general circulation models. *J. Climate*, **16**, 2653–2667, https://doi.org/10.1175/1520-0442(2003)016<2653: TSFMIT>2.0.CO;2.
- —, J. M. Wallace, and D. S. Battisti, 2003b: The seasonal footprinting mechanism in the Pacific: Implications for ENSO. *J. Climate*, 16, 2668–2675, https://doi.org/10.1175/1520-0442(2003) 016<2668:TSFMIT>2.0.CO:2.
- ——, M. A. Alexander, and M. Newman, 2014: Optimal growth of central and East Pacific ENSO events. *Geophys. Res. Lett.*, 41, 4027–4034, https://doi.org/10.1002/2014GL059997.
- Walker, G. T., and E. W. Bliss, 1932: World weather V. Mem. Roy. Meteor. Soc., 4, 53–84.
- Wang, W., M. Chen, and A. Kumar, 2010: An assessment of the CFS real-time seasonal forecasts. Wea. Forecasting, 25, 950– 969, https://doi.org/10.1175/2010WAF2222345.1.
- Wilks, D. S., 2006: On "field significance" and the false discovery rate. J. Appl. Meteor. Climatol., 45, 1181–1189, https://doi.org/ 10.1175/JAM2404.1.
- ——, 2016: "The stippling shows statistically significant grid points": How research results are routinely overstated and overinterpreted, and what to do about it. *Bull. Amer. Meteor. Soc.*, 97, 2263–2273, https://doi.org/10.1175/BAMS-D-15-00267.1.
- Wu, X., Y. M. Okumura, and P. N. DiNezio, 2019: What controls the duration of El Niño and La Niña events? *J. Climate*, 32, 5941–5965, https://doi.org/10.1175/JCLI-D-18-0681.1.
- Xie, P., and P. A. Arkin, 1996: Analyses of global monthly precipitation using gauge observations, satellite estimates, and numerical model predictions. *J. Climate*, **9**, 840–858, https://doi.org/10.1175/1520-0442(1996)009<0840:AOGMPU> 2.0.CO;2.
- You, Y., and J. C. Furtado, 2017: The role of South Pacific atmospheric variability in the development of different types of ENSO. *Geophys. Res. Lett.*, 44, 7438–7446, https://doi.org/10.1002/2017GL073475.
- —, and —, 2018: The South Pacific meridional mode and its role in tropical Pacific climate variability. *J. Climate*, 31, 10141–10163, https://doi.org/10.1175/JCLI-D-17-0860.1.
- Yu, J.-Y., and S. T. Kim, 2011: Relationships between extratropical sea level pressure variations and the central Pacific and eastern Pacific types of ENSO. *J. Climate*, 24, 708–720, https://doi.org/10.1175/2010JCL13688.1.
- Zhang, H., A. Clement, and P. Di Nezio, 2014: The South Pacific meridional mode: A mechanism for ENSO-like variability. *J. Climate*, 27, 769–783, https://doi.org/10.1175/JCLI-D-13-00082.1.
- Zhang, W., S. Li, F.-F. Jin, R. Xie, C. Liu, M. F. Stuecker, and A. Xue, 2019: ENSO regime changes responsible for decadal phase relationship variations between ENSO sea surface temperature and warm water volume. *Geophys. Res. Lett.*, 46, 7546–7553, https://doi.org/10.1029/2019GL082943.

- Zhao, J., M.-K. Sung, J.-H. Park, J.-J. Luo, and J.-S. Kug, 2023a: Part I observational study on a new mechanism for North Pacific Oscillation influencing the tropics. *npj Climate Atmos. Sci.*, 6, 15, https://doi.org/10.1038/s41612-023-00336-z.
 - —, —, —, and —, 2023b: Part II model support on a new mechanism for North Pacific Oscillation influence on ENSO. *npj Climate Atmos. Sci.*, **6**, 16, https://doi.org/10.1038/s41612-023-00337-y.
- Zhao, S., F.-F. Jin, and M. F. Stuecker, 2021: Understanding lead times of warm water volumes to ENSO sea surface temperature anomalies. *Geophys. Res. Lett.*, **48**, e2021GL094366, https://doi.org/10.1029/2021GL094366.
- Zuo, H., M. A. Balmaseda, S. Tietsche, K. Mogensen, and M. Mayer, 2019: The ECMWF operational ensemble reanalysis–analysis system for ocean and sea ice: A description of the system and assessment. *Ocean Sci.*, 15, 779–808, https://doi.org/10.5194/os-15-779-2019.